

Predicting the end of lava flow-forming eruptions from space

Estelle Bonny^{1,2}  · Robert Wright¹

Received: 21 September 2016 / Accepted: 23 May 2017 / Published online: 14 June 2017
© Springer-Verlag Berlin Heidelberg 2017

Abstract Although the volcanological community places great emphasis on forecasting the onset of volcanic eruptions, knowing when an effusive eruption will end is just as important in terms of mitigating hazards. Wadge (J Volcanol Geotherm Res 11:139–168, 1981) postulated that the onset of an episodic, lava flow-forming basaltic eruption is characterized by a rapid increase in effusion rate to a maximum, before decaying over a longer period of time until the eruption ends. We used thermal infrared remote-sensing data acquired by NASA's MODerate Resolution Imaging Spectroradiometer (MODIS) to derive time-averaged discharge rate (TADR) time series using the method of Harris et al. (J Geophys Res 102(B4):7985–8003, 1997) for 104 eruptions at 34 volcanoes over the last 15 years. We found that 32 eruptions followed the pattern described by Wadge (J Volcanol Geotherm Res 11:139–168, 1981). Based on the MODIS-derived maximum lava discharge rate and a decay constant that best fits the exponential waning phase (updated as each new MODIS TADR observation is added to the time series), the time at which the discharge equals zero, and thus the point at which effusion ends, can be predicted. The accuracy of the prediction improves with the number of data points so that, in the ideal case, the end of effusion can be retro-casted before half of the eruption duration has passed. This work demonstrates the possibility of predicting when an eruption will end using satellite-

derived TADR time series acquired in near real time during that eruption. This prediction can be made after an eruption has reached its maximum lava discharge rate and the waning phase of the Wadge trend has begun. This approach therefore only applies to the case of eruption from a chamber undergoing an elastic release of energy during lava flow emplacement, and we provide examples of eruptions where it would not be applicable.

Keywords Prediction · End-of-eruption · Effusive eruption · Discharge rate · MODIS

Introduction

The volcanological community has focused much attention on predicting when an eruption will begin (Linde et al. 1993; Sparks 2003; Marzocchi and Woo 2007; Marzocchi and Bebbington 2012; Pallister et al. 2013), mainly taking cues from seismicity (Harlow et al. 1996; Brenguier et al. 2008), ground deformation (Voight et al. 1998; Segall 2013), thermal emissions (Pieri and Abrams 2005; van Manen et al. 2013), or gas emissions (Baubron et al. 1991; Aiuppa et al. 2007). However, accurately forecasting when an eruption will end is similarly important in terms of hazard mitigation. This is especially true for lava flow-forming eruptions that can threaten population centers built down slope of vents. For example, accurate forecasting could help in terms of evacuation management allowing decisions to be made as when it is likely going to be safe for people to move back to their homes. Although, much more research has been conducted on forecasting eruption onset than eruption cessation, the recent work of Hooper et al. (2015) is a notable example of effort to forecast the end of an eruption (Bárðarbunga 2014–2015) using deformation measurements. Attempts to use satellite data to

Editorial responsibility: A. Harris

✉ Estelle Bonny
ebonny@hawaii.edu

¹ Hawaii Institute of Geophysics and Planetology, University of Hawaii, Honolulu, USA

² Department of Geology and Geophysics, University of Hawaii, Honolulu, USA

define (but not predict) the end of an effusive eruption have also been carried out, such as Aries et al. (2001) who showed that advanced very high-resolution radiometer (AVHRR) 3.9 μm radiance undergoes a sharp decline at the cessation of effusion. This can be used as a proxy for eruption termination and is due to the fact that exposure of the highly radiant flow interior through cracks in the flow surface ends when the flow is no longer moving.

Here, we present a method for using satellite-based infrared data, acquired in near real time during lava flow-forming eruptions, to predict when such eruptions will end. Wadge (1981) suggested that lava effusion rate (instantaneous volume flux of lava, in m^3/s) during effusive basaltic eruptions, when plotted against time, follows a typical asymmetric trend (Fig. 1). Wadge explained this temporal evolution in effusion rate in terms of rapid increase in lava flux after the onset of an eruption, with maximum lava discharge rate reached within the first few hours to days. This period of waxing flow is due to release of the magma chamber overpressure and gas exsolution. Effusion rate then decreases logarithmically over the rest of the eruption period due to the elastic release of energy from the magma chamber as it re-equilibrates with the lithostatic pressure. This simple logarithmic decay of volume flux with time is expressed as a relationship between the effusion rate at any time during the eruption ($Q_{f,t}$), the maximum lava discharge rate (Q_{max}), and a decay constant (λ) by

$$Q_{f,t} = Q_{\text{max}} e^{-\lambda t}, \quad (1)$$

as shown in Fig. 1. This typical asymmetric trend in effusion rate, hereafter referred to as a “Wadge curve,” has been recognized during many eruptions, including effusive events at Etna and Krafla (Harris et al. 1997, 2000), Nyamuragira, Piton

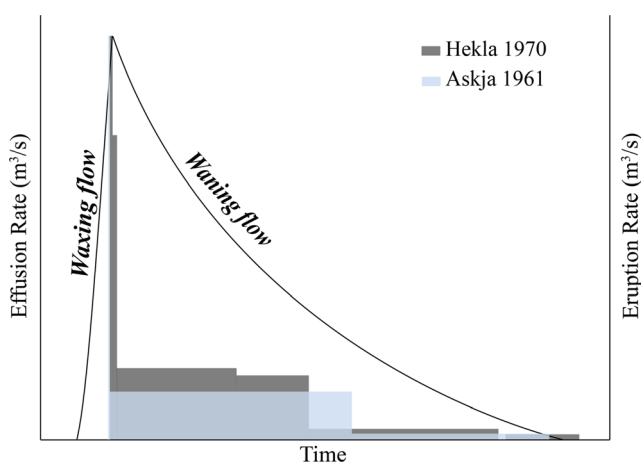


Fig. 1 Wadge (1981) theoretical model (black solid line) and two examples of his limited dataset from Hekla (1970) and Askja (1961). He used eruption rates (volume of lava erupted during a certain period of time and divided by that time) to approximate the variation of effusion rate due to the insufficient number of effusion rate measurements available at this time

de la Fournaise, and Sierra Negra (Wright and Pilger 2008). However, Coppola et al. (2017) and Harris et al. (2000, 2011), pointed out that at Piton de la Fournaise and Etna, respectively, this asymmetric trend does not occur for all effusive eruptions. The work described here assumes that most effusive lava flow-forming eruptions exhibit this relatively simple behavior, and that fitting a synthetic curve with the form of Eq. 1 to an effusion rate time series acquired during the waning phase (i.e., after the point of maximum discharge) will allow prediction of the end of the eruption (i.e., predicting when the lava discharge rate approaches zero). Crucially, our method uses effusion rate time series constructed from multi-temporal thermal infrared satellite measurements. As these measurements can be made as often as several times per day during eruptions anywhere on Earth, the end of an eruption can be predicted in near real time relatively soon after eruption onset, and updated as the eruption progresses and more satellite data are acquired.

We note, here, that infrared satellite data do not yield the instantaneous effusion rate, but instead yield a time-averaged discharge rate (TADR, Wright et al. 2001a; Harris and Baloga 2009; Harris 2013). Following Harris et al. (2007), lava effusion rate is defined as the instantaneous measure of lava flux from a vent at any given time, whereas TADR is the volumetric output averaged over some longer time period. Ultimately, the TADR becomes the mean output rate (MOR) if estimated at the end of an eruption from the total volume of erupted lava over the entire eruption duration. Here, we assume that our maximum TADR derived from the satellite data is equivalent to the maximum lava discharge rate defined by Wadge (1981; i.e., Q_{max}). We have used satellite-based TADR measurements made over the last 15 years to test how well such a method could work. Specifically, we used data acquired by the MODerate Resolution Imaging Spectroradiometer (MODIS) instruments, which have been operational since December 1999 (on NASA’s Terra satellite), and since May 2002 (on NASA’s Aqua satellite). This archive yields data for 104 effusive basaltic eruptions at 34 different volcanoes (Fig. 2).

Methods

Estimating time-averaged discharge rate from infrared satellite data

We used MODIS satellite data from both the Terra and Aqua spacecraft, focusing on data from a single thermal infrared channel with a central wavelength at 11.03 μm (band 31). MODIS band 31 spectral radiance data for any hot-spot detected by MODVOLC (Wright et al. 2002) are freely accessible online (<http://modis.higp.hawaii.edu>), and it is this database that we use. MODIS samples spectral radiance from the Earth’s surface in the thermal infrared (Fig. 3) with

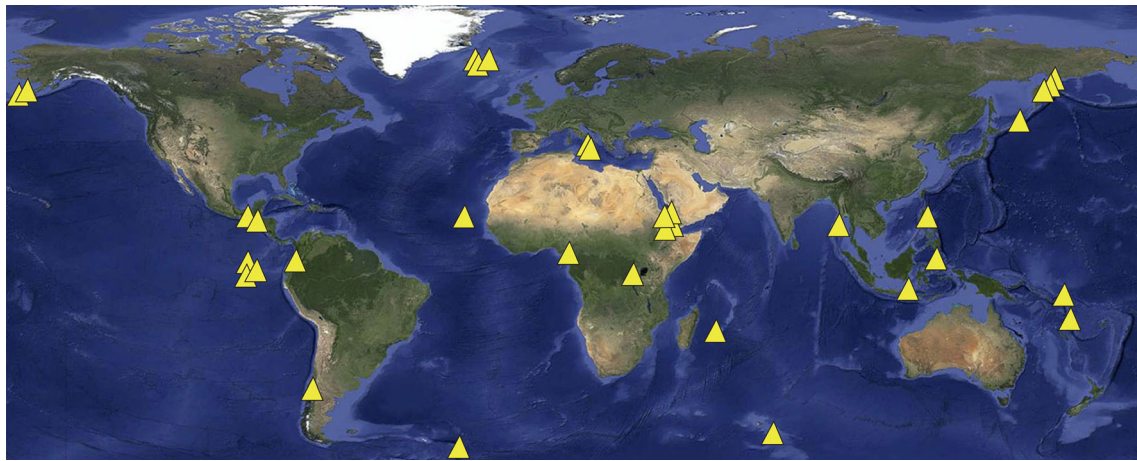


Fig. 2 Map of the 34 volcanoes where MODIS detected at least one effusive basaltic eruption in the last 15 years (for the period 2000–2014, inclusive)

an instantaneous field of view (IFOV) equivalent to 1 km^2 on the ground at nadir (although this increases to about $2 \times 5 \text{ km}$ at the edge of the $\sim 2500\text{-km}$ -wide sensor field of view).

TADR is estimated by applying the method from Harris et al. (1997, 1998, 2000, 2007) to the satellite spectral radiance, which is, in turn, based on the work of Pieri and Baloga (1986) who found a direct proportionality between lava discharge rate and the surface area of the resulting active lava flow. At-satellite spectral radiance in band 31 must be corrected for atmospheric effects (i.e., transmission losses as the signal passes upwards through the atmosphere, and an upwelling radiance component that the atmosphere itself emits towards the sensor) and surface emissivity. The corrected spectral radiance ($L_{11, \text{cor}}$) is an estimate of the spectral radiance leaving the ground surface contained within each

pixel. A two-component radiance mixture model, in which each pixel is assumed to contain a fraction of active lava surrounded by a colder background (representing the ground over which the active lava is flowing), is employed. To estimate the area of active lava within each pixel, the temperature of the lava flow surface, T_{lava} , must be assumed and Harris et al. (1997) use $100 \text{ }^\circ\text{C}$ as a lower estimate of the likely average temperature of an active lava flow surface (a cold case) and $500 \text{ }^\circ\text{C}$ as a likely upper estimate (a hot case).

For the background temperature, T_{back} , we use the approach of Wright et al. (2015), rather than that of Harris et al. (1997). T_{back} is estimated for each volcano in our dataset using the MODIS land surface temperature (LST) product. This product (MOD11C3 and MYD11C3 for Terra and Aqua, respectively) is downloadable from <https://search.earthdata.nasa.gov/> and takes the MOD11C1 and MYD11C1 daily global LST data set and computes a monthly average surface temperature for every 0.05° latitude/longitude (points are 5.6 km apart at the equator), after excluding cloudy values (via the MODIS cloud product). We then use each monthly average temperature value to compute a decadal average (2000–2010 for Terra and 2002–2012 for Aqua) for each point on the Earth's surface. For each calendar month, surface temperature averages were quantified for each MODIS overpass time (i.e., MODIS Aqua and Terra nighttime and daytime datasets), which produces a T_{back} robust to seasonal variations in surface temperature and cloud contamination.

How many eruptions conform to the idealized effusion rate behavior described by Wadge (1981)?

We examined the TADR time series of each eruption in our dataset (Fig. 2) to determine which ones displayed the waxing/waning trend defined by Wadge (1981). The relatively simple logarithmic decay that occurs during the waning phase of basaltic effusive eruptions enables us to compare the Wadge (1981) model to our satellite-derived time-averaged discharge

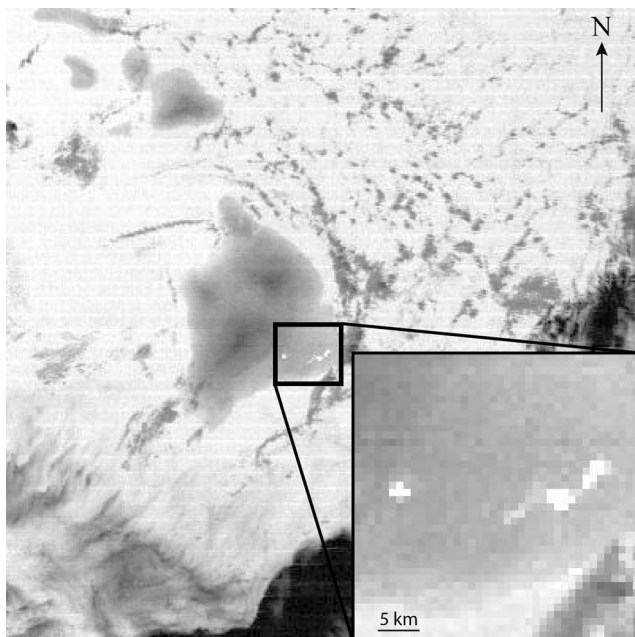


Fig. 3 MODIS Terra image of the Big Island on October 3, 2014 at 08:45 UTC from band 21

rates. More than simply visualizing each time series, we modeled a Wadge curve to compare the model with our space-based observations. We rearrange Eq. 1 to derive the time decay constant λ and to estimate a Wadge curve following

$$\lambda = \ln \left(\frac{0.1\% Q_{\max}}{Q_{\max}} \right) / t_{\text{end}}. \quad (2)$$

In this case, the only required values are the maximum lava discharge rate Q_{\max} and the time of the end of eruption (t_{end}) taken as the last TADR measurement calculated from our thermal infrared satellite data (Fig. 4). This approach is only possible when t_{end} is known, i.e., when the effusion has already ended, which does not enable the creation of a predictive tool. A technique for prediction will be described in the “How soon after the maximum lava discharge rate is attained can we predict the end of an effusive eruption?” section. Due to the asymptotic behavior of logarithmic decay, defining the end of the eruption is challenging. For consistency throughout, we considered the eruption to have ended when the time-averaged discharge rate reached a critical value (Q_{end}), selected to be 0.1% of the maximum lava discharge rate Q_{\max} . This cutoff was found to be representative of the time at which eruptions in our data set ended (i.e., the TADR after which radiance from the flow surface was insufficient to generate a detectable thermal anomaly). Choosing this value normalizes each eruption threshold to its maximum lava discharge rate and therefore varies for different eruptions and volcanoes. Thermal infrared TADR data can be calculated using the hot case ($T_{\text{lava}} = 500 \text{ }^\circ\text{C}$) or the cold case ($T_{\text{lava}} = 100 \text{ }^\circ\text{C}$). Since the critical limit is a percentage of Q_{\max} , the estimated decay constant is equal in both cases, and only the hot case is used in this study.

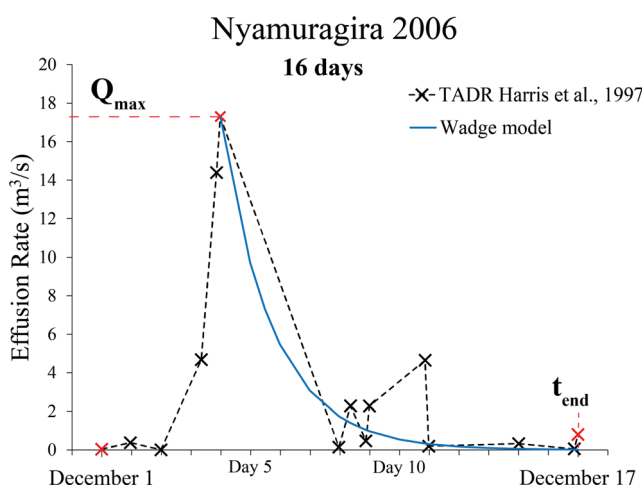


Fig. 4 Example of satellite-derived TADR time-series from Nyamuragira eruption in 2006 that displays a Wadge-type curve, illustrating the maximum lava discharge rate Q_{\max} and the last MODIS measurement that defines the end of the eruption (t_{end})

If the modeled Wadge curve (as calculated from Eq. 2) followed the satellite data in a given eruption, it was called a Wadge-type eruption (Fig. 5a). If the modeled curve was higher than the MODIS-derived discharge rate during the entire eruption and also exhibited a plateau of low TADR after about half of the eruption duration, it was classified as a half-Wadge-type eruption (Fig. 5b). We distinguished another group of eruptions having more than one maximum lava discharge rate (usually two), but still showing a logarithmic decay behavior that we called “double-pulse” type (Fig. 5c). All other eruptions were classified as undefined because no trend was visible and/or the TADR actually increased towards the end of the eruption (Fig. 5d). This increase was previously noticed by Wadge (1981) for some episodes at Kīlauea, which can be explained for this open-vent system by the backflowing of lava freezing the conduit resulting in lava pouring out for a longer period. All 104 eruptions in our dataset were placed in one of these four groups (Figs. 5 and 6), and only a third of the total conformed to the idealized Wadge-type eruption.

How soon after the maximum lava discharge rate is attained can we predict the end of an effusive eruption?

For Wadge-type eruptions, the simple decay trend of the waning phase can be exploited to predict the end of an eruption. We predict when our end-of-eruption criterion is met (i.e., $Q_{\text{end}} = 0.1\%$ of Q_{\max}) by fitting an exponential function (following Eq. 1) to our TADR time series. We estimate the decay constant that best fits the waning phase of the eruption based only on our MODIS-derived satellite data with no “a priori” knowledge of the time at which the eruption ended (t_{end}). Once the maximum lava discharge rate had been reached (i.e., the eruption has entered its waning phase) the time at which TADR falls below the cessation criteria is predicted using only the MODIS data available at that time and compared to the known end date of the eruption. Clearly, few data are available at first. As the eruption progresses, and new satellite data become available, we update the best-fit decay constant as new MODIS TADR observations are added to the time series (i.e., the amount of data available to constrain the prediction increases with time). By re-computing each time a new TADR is added to the time series, we are able to simulate how the method would work in near real time during an eruption.

Our results are expressed in two ways. First, we determine how the prediction of effusion cessation evolves as the amount of TADR data used to compute the prediction increases. Specifically, once Q_{\max} was observed, we progressively add roughly 10% of the total TADR data to the time series, and fit a new exponential curve to our satellite measurements each time (e.g., 10% of the data, 20, 30, up to 100%). For each “data step,” the predicted end ($t_{\text{end, pred}}$) is then defined as the time at which the TADR reaches the critical value (Q_{end})

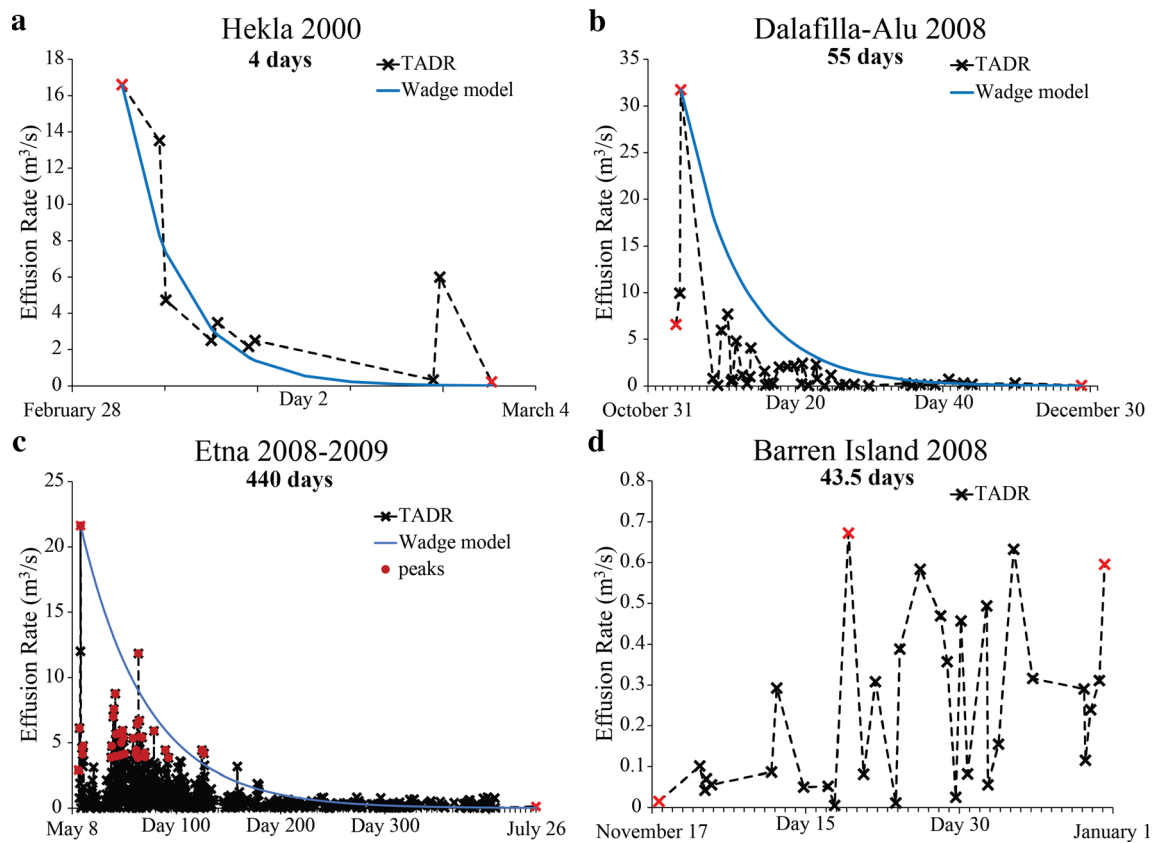


Fig. 5 Examples of different TADR time-series with the Wadge model curve drawn for comparison. **a** Wadge type, **b** half-Wadge, **c** double pulse, **d** undefined

and compared (in terms of days) with the observed eruption end (t_{end}) corresponding with the last TADR data point detected by MODIS. Second, we express our predictions in terms of percent of eruption duration, which allows for a simpler comparison between eruptions since the TADR measurements are not acquired at regular intervals, or equally spaced in time (e.g., 50% of the total TADR observations after Q_{max} does not always equal 50% of the eruption duration). The best fit of our data was found in a least-square sense (difference

squared between the exponential curve and the satellite data). The difference between the predicted end and the observed end is expressed in terms of Δt (in days or % eruption duration) for each time at which a new TADR estimate is added to the time series:

$$\Delta t = t_{end,pred} - t_{end} \tag{3}$$

Δt is positive when the predicted cessation is after the observed end of effusion and negative when it predates the observed end. Figure 7 provides an illustration of the method where Δt_{20} is a schematic representation for the Δt that is predicted using 20% of the TADR data.

After the initial TADR calculation, we account for possible cloud contamination. Sub-pixel clouds are hard to identify and can cause low at-satellite spectral radiance, which produces an artificially low TADR estimate. For the eruptions in our dataset that have a well-defined TADR time series (i.e., a large amount of data available), we attempt to exclude some cloud-contaminated values by only selecting the peak TADR measurements, or local maxima in discharge rate, that are one standard deviation above the median of all such local maxima (one-*nsig* criterion). In some cases, this greatly reduces the number of data points available for prediction (sometimes to as few as two TADR observations), and in this case, we use all

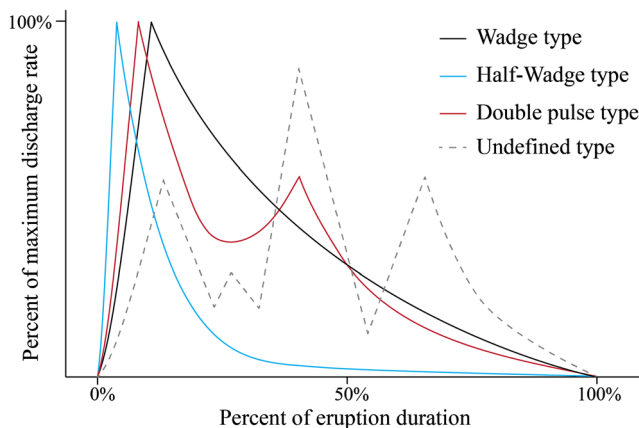


Fig. 6 Schematic of different lava discharge rate time-series types

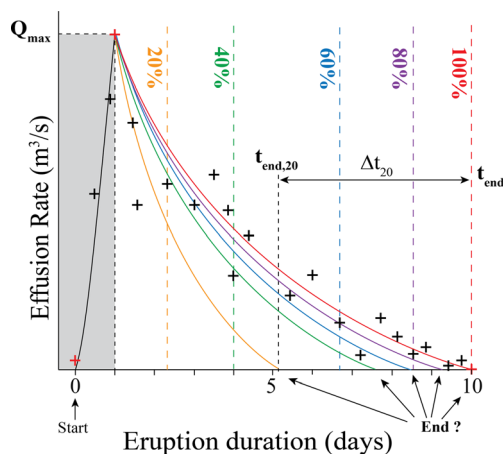


Fig. 7 Cartoon of the method used for predicting the end of the eruption in this paper. The colors of each exponential curve represent a different fit of a given amount of data (in percent) and give a different predicted end, with the associated Δt (Δt_{20} represents the Δt that is predicted using 20% of the TADR data). The red crosses represent three important points: the first is the onset of the eruption, the second is the maximum lava discharge rate, and the last is the last TADR data point or the observed eruption end t_{end} . All of the data above are thermal infrared remote-sensing data from MODIS. Notice that the fit with 40% of the data (green line) after Q_{max} is equal to 40% of the eruption duration but this is not always the case

TADR estimates classified as “peaks.” For other eruptions, mainly those of short duration, the amount of TADR available can be so limited that no cloud-screening is feasible and all TADR estimates are used.

Results

Of the 104 eruptions studied, 32 eruptions strictly followed the typical Wadge curve, eight exhibited a double pulse in TADR, 13 corresponded to a half-Wadge type, and 51 were undefined and did not show any trend at all (Fig. 5). Of the 32 eruptions, only half could be used (the remainder comprised of fewer than five TADR data points) and our predictions are summarized in Table 1. The table shows the evolution of the prediction for each eruption, as we increased the amount of TADR estimates available and updated the best-fit exponential curve. Although, we have divided the time series into percentiles of data used to compute the curves, far more relevant is how soon after the eruption began can the end-of-eruption prediction be made, and how good is that prediction. For this reason, Table 1 gives both measures: Δt , both in terms of days and percent of eruption duration; and the time since the onset of eruption at which the prediction could be made (also in terms of days and percent of eruption duration). For example, to illustrate how the data in the table are to be interpreted, in the case of the Piton de la Fournaise eruption of December 2005, our best prediction (bold in the table) was that the eruption would last 9 days (it lasted 10 days, for a Δt of -1). This prediction would have

been possible on day 3 of the eruption (or after 30% of eruption duration had elapsed) at which time 30% of the MODIS data that would ultimately define the total TADR curve for the eruption had been acquired. For the Kizimen eruption of 2011, a good prediction (Δt within 7%) is possible on day 47 (or after 22% of the eruption had passed, at which time 70% of the MODIS data had been acquired) that the eruption would last 198 days (it lasted 212 days, for a Δt of -14 days). And if we had waited until 48% of the eruption had elapsed (day 102), our best prediction was that the eruption would last 211 days which is within 1% of the actual eruption duration. At this time, 90% of the MODIS data that would ultimately define the TADR curve for the eruption had been acquired.

To illustrate the viability of our predictive tool, we concentrate on three case studies: one eruption of short duration from Piton de la Fournaise in December 2005, one of medium duration from Nyamuragira in 2000, and one of long duration from Kizimen in 2011. For each graph shown (Figs. 8, 9, and 10), the green horizontal line represents the critical limit, Q_{end} that defines the end of the eruption. Figs. 8, 9, and 10 all include an inset figure, which summarizes how the end-of-eruption prediction changes (i.e., improves as we move up and closer to a Δt of zero along the y-axis) as we use more satellite data to constrain the prediction (i.e., as the eruption progresses, moving right along the x-axis). The more rapidly the curve in this figure approach a Δt of zero, the better.

Piton de la Fournaise 2005

Piton de la Fournaise is a stratovolcano located in La Reunion Island, in the Indian Ocean. MODIS detected a lava-producing eruption that started on December 26, 2005 and ended on January 4, 2006, for a total duration of 10 days. The maximum lava discharge rate was reached on December 27 at 20:49 UTC about a day after the eruption started with a TADR of $8 \text{ m}^3/\text{s}$ (Fig. 8). Since we only have 15 satellite TADR measurements during the waning phase, we decided to keep every data point to apply our predictive tool.

Once two measurements after Q_{max} were obtained, in this case 1.5 days after the onset of the eruption (here 15% of the eruption duration), we began fitting an exponential curve to our data, which predicted that the eruption would last only 3 days instead of the observed 10 days (Δt of -7 days, dark blue diamond in Fig. 8f inset). After adding three more TADR estimates 3 days past the onset of the eruption, our method predicted that the eruption would last 9 days, which is accurate to within 1 day of the observed end of eruption ($\Delta t = -1$ day, light blue in Fig. 8f inset). This new prediction was 6 days closer to the observed end than the prediction made with two data points and happened to be the most accurate prediction after 30% of the eruption duration had elapsed. Using data from 4 days after the eruption onset, we predicted that the eruption would last 8 days; in fact, it lasted 10 days ($\Delta t = -2$ days, purple diamond

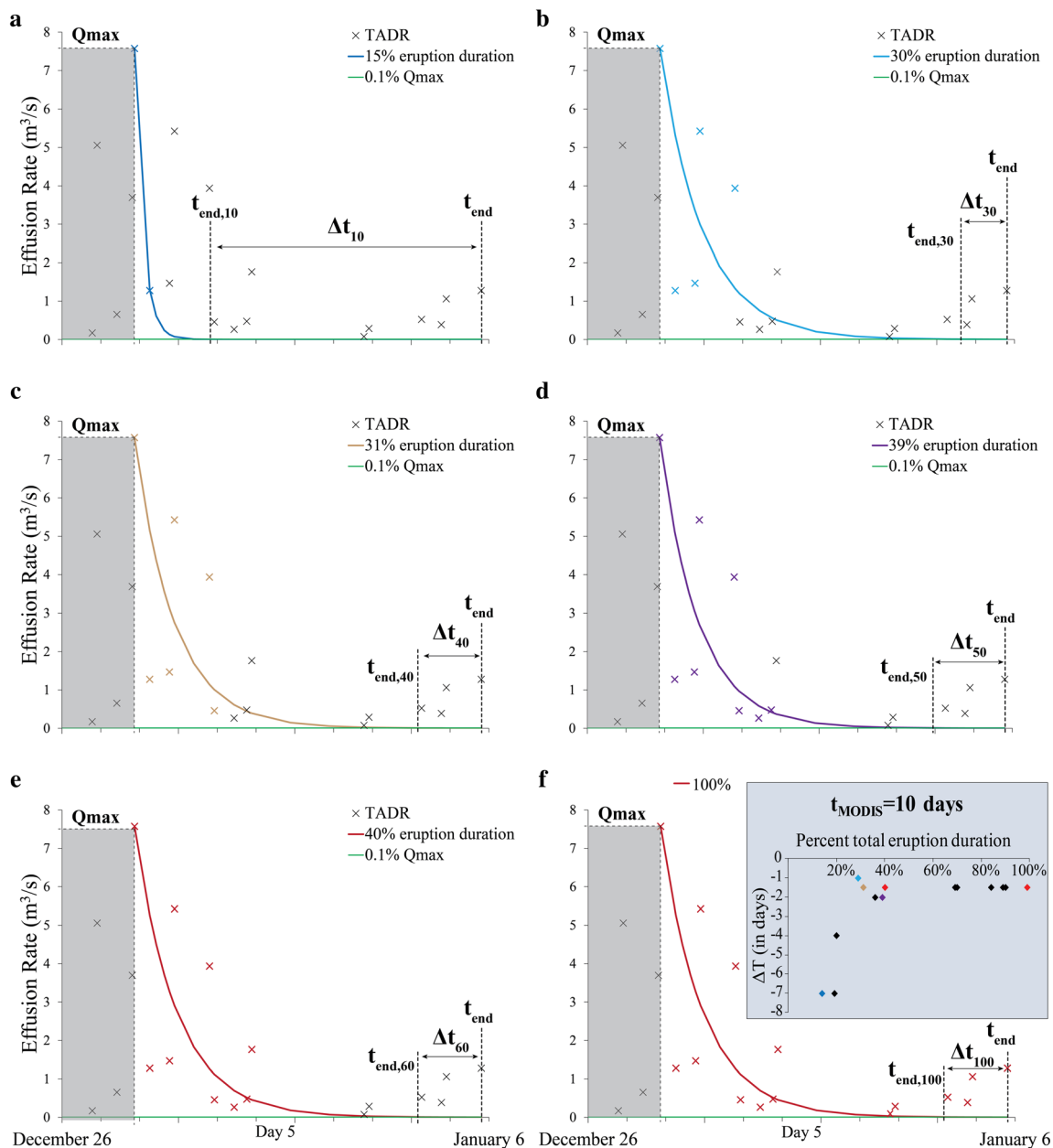


Fig. 8 The December 2005 eruption of the Piton de la Fournaise as observed by MODIS (eruption duration is 10 days). All axes have the same scale and legend. Δt_{10} represents the Δt that is predicted using 10% of the TADR data. **f** Inset shows the evolution of the prediction as we

increased the amount of data used to fit Eq. 1 (a–f; 15% eruption duration to 100%), and the colors of the TADR data points (*crosses*) and curves match to show which data were used to generate each prediction

in Fig. 8f inset). A few hours later, with one more TADR observations, we reached the best fit curve (same prediction with 100% data) which yielded an eruption that would end after 8.5 days (Δt of -1.5 days). As we increase the amount of TADR used and the eruption progresses, the prediction does not necessarily get better, but our best end-of-eruption prediction (within a day) could be estimated only 3 days after the eruption started (equivalent to 30% of the observed eruption duration). This result is significant in terms of hazard mitigation for this type of episodic basaltic eruption with a prediction of the eruption cessation 7 days in advance.

Nyamuragira 2000

Nyamuragira is a shield volcano in DR Congo, the most active volcano in Africa (Smets et al. 2010). An eruption was recorded by MODIS on February 25, 2000 that lasted until April 23, 2000, totaling 58 days. The eruption produced a lava flow, bombs, cinder, and ash (Global Volcanism Program 2000). The maximum lava discharge rate was detected on February 26 at 20:50 UTC only 1 day after the beginning of the eruption with a TADR of $17 m^3/s$ (Fig. 9). In this case, we used all the identified peaks to increase the amount of data available

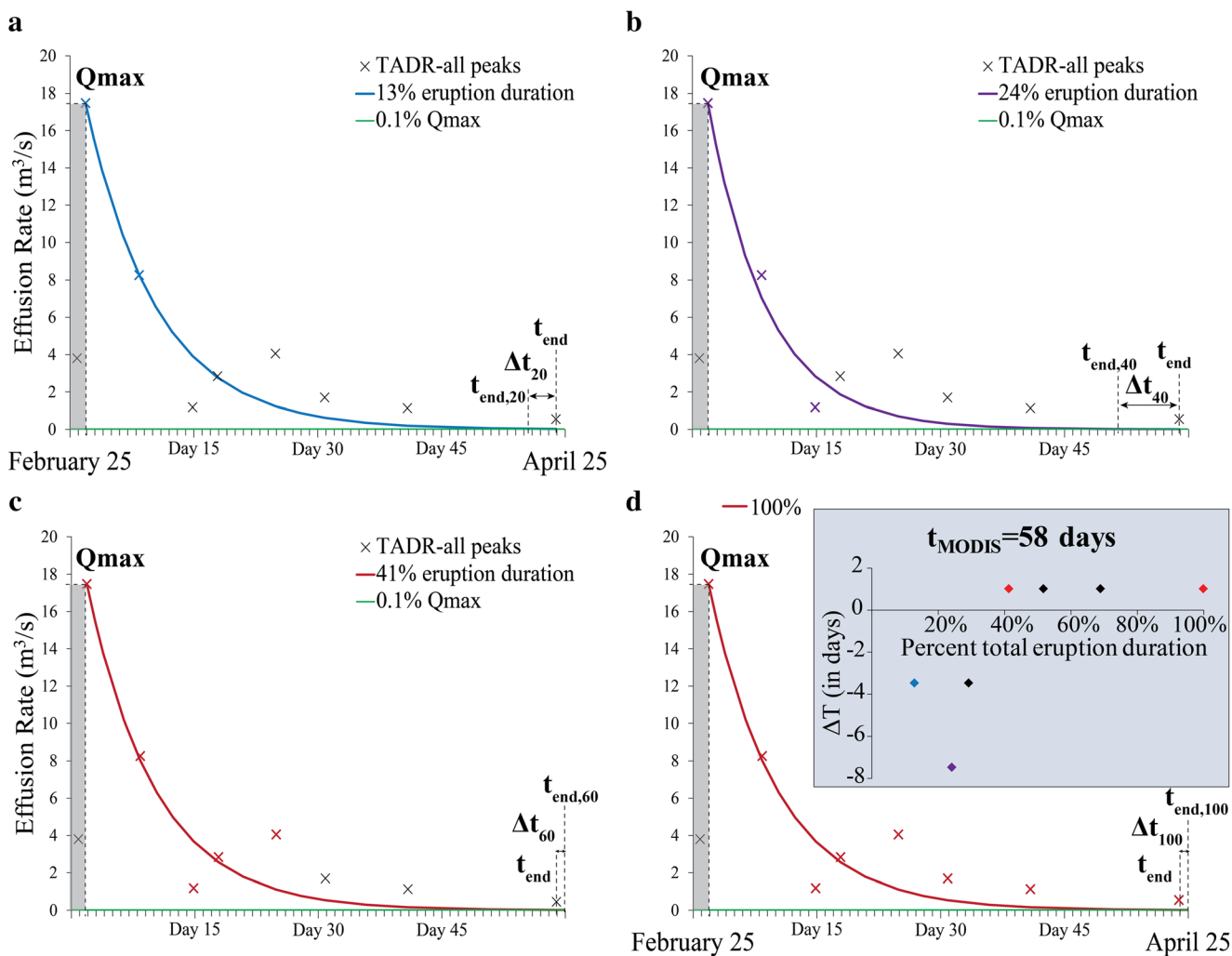


Fig. 9 The Nyamuragira 2000 eruption (with a duration of 58 days) TADR time-series as detected by MODIS. **d** Inset shows the evolution of the end of eruption prediction as we increased the amount of data used to fit Eq. 1 (a–d; 13 to 100% of eruption duration). All graphs have the

same scale and legend if not indicated and the colors of the TADR data points (crosses) and curves match to show which data were used to generate each prediction. Δt_{20} represents the Δt that is predicted using 20% of the TADR data

(proving us with 8 data points instead of the 3 points that would have been available had we enforced the one-*nsig* criterion).

For Nyamuragira, 7.5 days after the onset of the eruption (13% of the eruption duration), our method (with 25% of data or two TADR values) predicted that the eruption would last 54.5 days, close to the observed end ($\Delta t = -3.5$ days; blue diamond in Fig. 9d inset). However, 14 days after the onset of the eruption (with three TADR values or after 24% of the eruption duration had passed), we predicted that the eruption would end after 50.5 days ($\Delta t = -7.5$ days). Our best prediction (also the final estimate) was that the eruption would last 59 days and this was found after 24 days into the eruption (41% of eruption duration) at which time 60% of the MODIS data that would ultimately define the total TADR curve for the eruption had been acquired. The eruption actually lasted 58 days, 1 day before the predicted end ($\Delta t = 1$ day, red diamond in Fig. 9d inset). Therefore, for Nyamuragira, we have a good prediction

(Δt within 6%) a week into the eruption (i.e., after only 13% of the eruption had elapsed), and reached the most accurate prediction (to within 1 day) before half of the eruption had passed.

Kizimen 2011

Kizimen is a stratovolcano in Kamchatka, Russia, and we focused on the first phase of the eruption that started on March 1, 2011 and ended on September 29, 2011 (Global Volcanism Program 2011). In the second phase of this eruption (starting on October 3), the TADR time series did not exhibit the typical Wadge trend, so we only concentrated on the first phase to use our predictive tool. The first phase lasted 212 days and reached a maximum lava discharge rate on March 1 at 15:25 UTC, which is the first point that MODIS detected with a TADR of 12 m³/s (Fig. 10). During this long duration eruption, we retrieved many estimates of TADR that allowed us to use the identified peaks

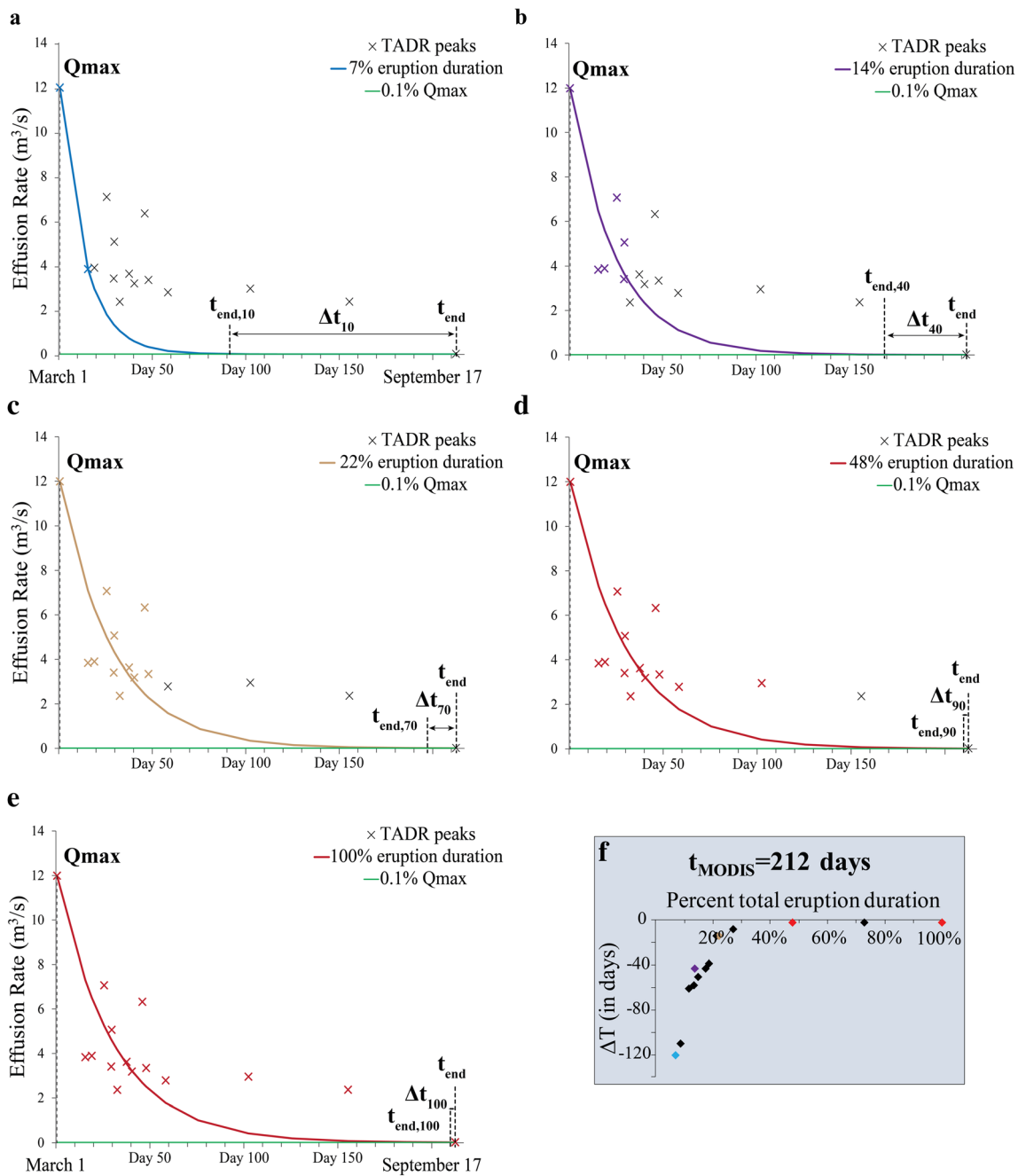


Fig. 10 The Kizimen 2011 eruption, phase 1 from March 1 to September 29. TADR were calculated from MODIS data and the eruption duration is 212 days. **f** Evolution of the end of eruption prediction as we increased the amount of data used to fit Eq. 1 (a–e; 7 to 100% of eruption duration). All

graphs have the same units and legend and the colors of the TADR data points (*crosses*) and curves match to show which data were used to generate each prediction. Δt_{10} represents the Δt that is predicted using 10% of the TADR data

(one-*nsig* criterion) as defined in the “How soon after the maximum lava discharge rate is attained can we predict the end of an effusive eruption” section (15 peaks were found).

For Kizimen, 15 days after the onset of the eruption or 7% of the eruption duration (with two TADR values) our method predicted that the eruption would last 91 days, which is about 4 months shorter than the observed duration of 212 days ($\Delta t = -121$ days, blue diamond in Fig. 10f). With six TADR

values (or 40% of data), we predicted that the eruption would end after 169 days; in fact, it lasted 212 days. This prediction would have been possible on day 29 of the eruption (or after 14% of eruption duration had elapsed) at which time 40% of the MODIS data that would ultimately define the total TADR curve for the eruption had been acquired. However, if we wait 19 more days (47.5 days after the eruption onset or 22% eruption duration), our method predicts that the eruption would last

Table 1 Summary of the 16 Wadge eruption predictions

| P. Fournaise December 2005 | | | Nyumuragira 2000 | | | Kizimen 2011 | | | Cameroon 2000 | | |
|----------------------------|-----------------|-----|------------------------|-----|-----|-------------------|-----|-----|------------------|-----|------|
| 10 days (a) | | | 58 days (p) | | | 212 days (n) | | | 48.5 days (a) | | |
| % data | Δt days | % | Δt days | % | % | Δt days | % | % | Δt days | % | % |
| 10 | -7 | -70 | 1.5 | 15 | 13 | -121 | -57 | 7 | -33 | -68 | 16.5 |
| 20 | -7 | -70 | 2 | 19 | 30 | -110 | -52 | 9 | -33 | -68 | 18.5 |
| 30 | -1 | -10 | 3 | 30 | 30 | -58 | -27 | 14 | -33 | -68 | 20.5 |
| 40 | -1.5 | -15 | 3 | 31 | 24 | -43 | -20 | 14 | -33 | -68 | 21 |
| 50 | -2 | -20 | 4 | 39 | 29 | -43 | -20 | 17 | -33 | -68 | 21 |
| 60 | -1.5 | -15 | 4 | 40 | 41 | -39 | -18 | 19 | -33 | -68 | 22.5 |
| 70 | -1.5 | -15 | 7 | 70 | 52 | -14 | -7 | 22 | -12.5 | -26 | 23 |
| 80 | -1.5 | -15 | 8.5 | 85 | 69 | -8 | -4 | 27 | -12 | -25 | 32 |
| 90 | -1.5 | -15 | 9 | 90 | 100 | -2 | -1 | 48 | -12 | -25 | 39 |
| 100 | -1.5 | -15 | 10 | 100 | 100 | -2 | -1 | 100 | -12 | -25 | 48.5 |
| Etna July 2001 | | | Etna Nov 2007 | | | Reventador 2007 | | | Stromboli 2007 | | |
| 21.5 days (a) | | | 1 day (a) | | | 62 days (a) | | | 34 days (p) | | |
| % data | Δt days | % | Δt days | % | % | Δt days | % | % | Δt days | % | % |
| 10 | -11.5 | -53 | 6 | 28 | 40 | -7.5 | -12 | 19 | -23.5 | -69 | 6 |
| 20 | -10 | -47 | 7.5 | 35 | 50 | -11 | -18 | 24 | -14.5 | -42 | 12 |
| 30 | -7 | -33 | 9 | 42 | 60 | -11 | -18 | 24 | -11.5 | -33 | 16 |
| 40 | -6 | -28 | 10.5 | 49 | 67 | -11 | -18 | 24 | -10 | -29 | 19 |
| 50 | -6 | -28 | 11.5 | 53 | 76 | -11 | -18 | 24 | -9 | -26 | 28 |
| 60 | -4 | -19 | 13 | 60 | 88 | -11 | -18 | 100 | -8 | -23 | 32 |
| 70 | -3.5 | -16 | 14.5 | 67 | 100 | -11 | -18 | 100 | -8 | -23 | 34 |
| 80 | -3.5 | -16 | 16.5 | 76 | | | | | | | |
| 90 | -3.5 | -16 | 19 | 88 | | | | | | | |
| 100 | -3.5 | -16 | 21.5 | 100 | | | | | | | |
| Hekla 2000 | | | Klyuchevskoy 2008-2009 | | | Llaima April 2009 | | | Nyumuragira 2006 | | |
| 4 days (a) | | | 67.5 days (n) | | | 10 days (a) | | | 16 days (a) | | |
| % data | Δt days | % | Δt days | % | % | Δt days | % | % | Δt days | % | % |
| 10 | 10 | 250 | 0.4 | 10 | 44 | -5.5 | -55 | 18 | -6 | -38 | 8 |
| 20 | 1 | 25 | 0.5 | 13 | 44 | -5 | -50 | 20 | -1.5 | -9 | 8.4 |
| 30 | 0.5 | 13 | 1 | 25 | 45 | -4.5 | -45 | 25 | -1.5 | -9 | 8.9 |
| 40 | 0.5 | 13 | 1 | 25 | 45 | -3 | -30 | 29 | 0 | 0 | 9 |
| 50 | 1 | 25 | 1 | 25 | 46 | 0 | 0 | 30 | 1.5 | 9 | 10.9 |
| 60 | 1 | 25 | 1.4 | 35 | 47 | 0.5 | 5 | 35 | 1.5 | 9 | 11 |
| 70 | 1 | 25 | 1.4 | 35 | 48 | 1.5 | 15 | 40 | 1.5 | 9 | 14 |
| 80 | 1 | 25 | 3.4 | 85 | 49 | 2 | 20 | 49 | 1.5 | 9 | 15.9 |
| 90 | 1 | 25 | 3.4 | 85 | 100 | 2.5 | 25 | 69 | 1.5 | 9 | 16 |
| 100 | 1 | 25 | 4 | 100 | | 2.5 | 25 | 100 | 1.5 | 9 | |

Table 1 (continued)

| % data | P. Fourmaise August 2004 61.5 days (<i>p</i>) | | | P. Fourmaise July 2006 21.5 days (<i>a</i>) | | | P. Fourmaise April 2007 29 days (<i>p</i>) | | | P. Fourmaise October 2010 21 days (<i>p</i>) | | |
|--------|--|-----|-----------------------------------|--|-----|-----------------------------------|---|------|-----------------------------------|---|-----|-----------------------------------|
| | Δt days | % | Time since eruption onset days | Δt days | % | Time since eruption onset days | Δt days | % | Time since eruption onset days | Δt days | % | Time since eruption onset days |
| 10 | -28.5 | -46 | 20 | -20.5 | -95 | 2 | -2 | -7.5 | 10.5 | -12.5 | -60 | 2 |
| 20 | -27 | -44 | 25 | -14 | 33 | 5.5 | -7 | -25 | 13 | -2 | -10 | 4 |
| 30 | -11.5 | -19 | 27.5 | 5 | 23 | 6 | -6 | -21 | 16.5 | 1 | -5 | 5 |
| 40 | -11.5 | -19 | 43.5 | 7 | 33 | 10.5 | -5 | -18 | 20.5 | 0 | 5.5 | 5.5 |
| 50 | -11.5 | -19 | 47.5 | 8 | 37 | 14.5 | -5 | -18 | 21.5 | 1.5 | 7 | 8.5 |
| 60 | -11.5 | -19 | 54.5 | 8 | 37 | 15.5 | -4.5 | -16 | 23.5 | 2.5 | 12 | 12 |
| 70 | -11.5 | -19 | 61.5 | 10.5 | 49 | 16.5 | -4.5 | -16 | 27 | 3.5 | 17 | 15.5 |
| 80 | -11.5 | -19 | 89 | 12 | 56 | 20 | -4.5 | -16 | 28.5 | 3.5 | 17 | 16 |
| 90 | -11.5 | -19 | 100 | 12 | 56 | 21.5 | 1 | 1 | 29 | 3.5 | 17 | 21 |
| 100 | -11.5 | -19 | 100 | 12 | 56 | 21.5 | 1 | 1 | 29 | 3.5 | 17 | 21 |

In bold is the “best” prediction (the smallest Δt) and in italic is a reasonably good prediction (the earliest prediction with a Δt at or less than 25% of the eruption duration), and in bold italic is when both the good and best prediction are happening at the same time. Δt is in days and in percent of the eruption duration. The same is given for the time since eruption onset at which the prediction could have been made (in days and in percent of the eruption duration). The empty cells are for non-available data. Each eruption uses different amount of TADR data to make our prediction and *a* stands for using all the TADR available without screening for low values, *p* is for all the available “peaks” TADR, and *n* is for the plus one-nsig criterion

198 days, which is accurate to within 14 days ($\Delta t = -14$ days or 7% the eruption duration, brown diamond in Fig. 10f) of the observed end. At 102 days after the eruption onset (about half the eruption duration), our method predicted that the eruption would end after 210 days which is 2 days from the observed end. The prediction does not change once we add more data to our method. This case study shows that after only 14% of the eruption had elapsed (day 29), the end of the effusion could be predicted with a 20% accuracy ($\Delta t = -20\%$ eruption duration, which represents 43 days before the observed end). However, if we wait until 22% of the eruption has passed, a highly accurate end-of-eruption prediction can be made with a Δt of -7%. And this could be improved to a 2-day offset in the prediction with half of the eruption duration.

Discussion and conclusions

Our initial goal was to determine a decay constant that best described all 104 eruptions in our dataset that would be “globally applicable” and then to use this global value to retro-cast the end of basaltic effusive eruptions. However, we observe too wide a range of decay constant values and thus a single average decay constant would not be valid for all eruptions. Focusing on a single volcano, the same issue arises: each eruption from a specific volcano has a unique TADR time-series trend that we cannot generalize (Harris et al. 2011; Coppola et al. 2017).

Using the ideal case defined by Wadge (1981), it is possible to predict in advance when effusion will cease if the waxing/waning behavior of the TADR time series follows this trend. One limitation of this technique is that it may not be obvious initially whether the eruption will exhibit the Wadge-type TADR behavior, although the satellite data themselves could be used to make this determination as the TADR curve is compiled. The method we present is also potentially useful for other types of eruption, like the double pulse. In this case, the predictions would simply be reset after the secondary TADR peak. The detection of the maximum lava discharge rate Q_{max} is of great importance, and missing it would prevent a reliable forecast, especially when there is inadequate data and no observations close to the true time of Q_{max} to compensate. How many of our time series were not classified as “Wadge-type” eruptions simply because MODIS did not sample the key maximum lava discharge rate? We experimented with what would happen when removing Q_{max} from our TADR time series for some eruptions in our dataset and observed three different outcomes: (i) the Wadge curve could not be defined anymore, (ii) the Wadge curve was still visible but the prediction was degraded, or lastly, and perversely, (iii) the prediction ameliorated. Improved temporal resolution of the satellite data

acquisitions (perhaps by merging data from multiple platforms) would help ameliorate this.

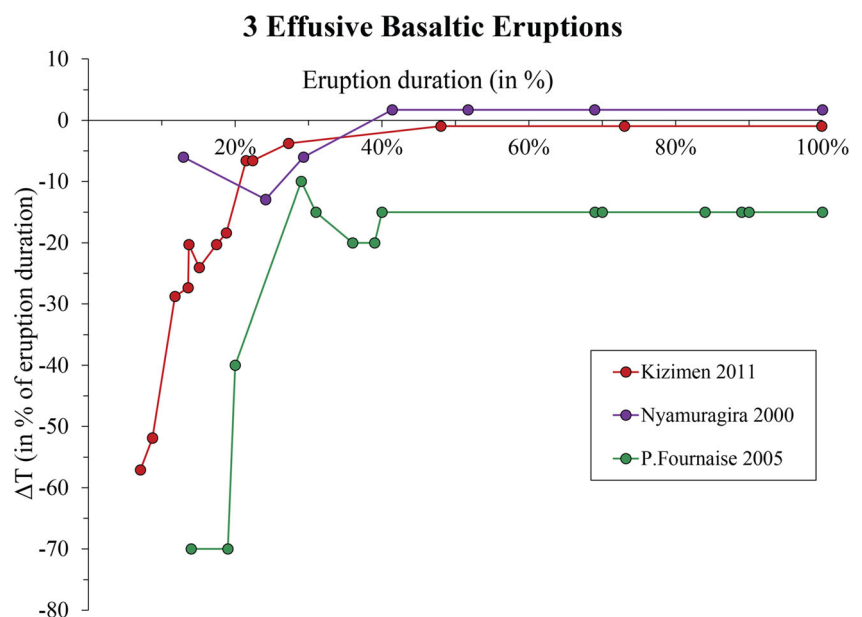
Another limitation arises from the thermal cooling behavior of a lava flow. Some lava flows can continue to radiate heat for a long period even after the flow has stopped advancing and can still be “hot” enough to be detectable by space-based sensors. The end of an eruption is therefore hard to define and often there is a discrepancy between the start and end date recorded depending on the techniques used, e.g., satellite measurements, the Global Volcanism Program database and literature on specific eruptions. For consistency throughout this work, we decided to use only our thermal infrared remote-sensing data for reference in our predictive tool. However, the work of Aries et al. (2001) and Wright et al. (2001b) shows that precipitous decreases in emitted short-wave and mid-wave infrared (SWIR and MWIR, respectively) radiance accompany the time at which an active lava flow stops moving. In short, when the flow stops moving fresh cracks on the flow surface (which expose the hotter flow interior that contribute greatly to the observed SWIR and MWIR radiance) are not created to replace cooling lava in older cracks. As such, defining the end of an eruption using thermal infrared satellite data should be somewhat robust provided the detection method using the SWIR or MWIR spectral intervals.

The TADR that marks the end of eruption has been assumed arbitrarily as 0.1% of the maximum lava discharge rate since it works best for most of the Wadge type eruptions. But one can argue that a fixed value should be used at all time, such as the 2–3 m³/s that Wadge mentioned in his 1981 paper. But with technologic advancements, it is now possible to resolve much lower values of discharge rates so

we decided on a lower critical value. In Table 1, we summarize all the predictions made with the method described here. To generalize our estimates for all the eruptions, we relied on the estimate of Δt in percent of the eruption duration. We found that the end of an eruption could be predicted (to within Δt of 25% of the observed duration) as early as 13% after it begins, and no later than 94% (Fig. 11 shows a summary of our three case studies). Each data point shows how the residual between the predicted end and the actual end of the eruption changes (moving “up” along the y -axis, as a percent of eruption duration) as more data are available to compute the prediction (i.e., after eruption onset, expressed as percent of eruption duration). Obviously, the more rapidly the curve approaches a ΔT of zero, the sooner after eruption onset the end of eruption can be predicted. The closer the curve approaches the ΔT of zero, the more accurate that prediction is. Generally, less than half of the eruption duration (average of 43%) allows for our best prediction. It can be seen that TADR time series have peaks and troughs and therefore the prediction of the end of effusion does not always improve with time.

In summary, once an effusive eruption starts, and the TADR time series conforms to the Wadge type, we can use thermal infrared satellite remote-sensing data to predict the cessation of effusion with high accuracy before the eruption is half over and with reasonable accuracy even earlier after the eruption onset. In the future, applying this technique to an ongoing eruption in real time, instead of retrospectively, would be of great interest for lava flow hazard mitigation. Its key contribution would be to reduce the damaging uncertainty that results from not knowing when multi-month-long lava flow eruptions will end.

Fig. 11 Summary for the three episodic basaltic effusive eruptions detected by MODIS discussed in detail in this paper. Both axes are in percentage of eruption duration to allow for a comparison in the prediction



Acknowledgements EB and RW were funded by NASA (NNX14AP34G and NNX14AP37G). Harold Garbeil and Eric Pilger (HIGP) provided programming support and Pete Mouginiis-Mark (HIGP) provided some helpful insights. The manuscript benefited from reviews by Andy Harris and an anonymous reviewer. This is HIGP publication 2252 and SOEST publication 9909.

References

- Aiuppa A, Moretti R, Federico C, Giudice G, Gurrieri S, Liuzzo M, Papale P, Shinohara H, Valenza M (2007) Forecasting Etna eruptions by real-time observation of volcanic gas composition. *Geology* 35(12):1115–1118. doi:10.1130/G24149A.1
- Aries SE, Harris AJL, Rothery DA (2001) Remote infrared detection of the cessation of volcanic eruptions. *Geophys Res Lett* 28(9):1803–1806
- Baubron JC, Allard P, Sabroux JC, Tedesco D, Toutain JP (1991) Soil gas emanations as precursory indicators of volcanic eruptions. *J Geol Soc Lond* 148:571–576
- Brenguier F, Shapiro NM, Campillo M, Ferrazzini V, Duputel Z, Coutant O, Nercessian A (2008) Towards forecasting volcanic eruptions using seismic noise. *Nat Geosci* 1:126–130. doi:10.1038/ngeo104
- Coppola D, Di Muro A, Peltier A, Villeneuve N, Ferrazzini V, Favalli M, Bachèlery P, Gurioli L, Harris AJL, Moune S, Vlastélic I, Galle B, Arellano S, Aiuppa A (2017) Shallow system rejuvenation and magma discharge trends at Piton de la Fournaise volcano (la Réunion Island). *Earth Planet Sci Lett* 463:13–24
- Global Volcanism Program (2011) Report on Kizimen (Russia). In: Wunderman R (ed) *Bull Glob Volcanism Netw* 36:10. Smithsonian Institution. doi:10.5479/si.GVP.BGVN201110-300230
- Global Volcanism Program (2000) Report on Nyamuragira (DR Congo). In: Wunderman R (ed) *Bull Glob Volcanism Netw* 25:1. Smithsonian Institution. doi:10.5479/si.GVP.BGVN200001-223020
- Harlow DH, Power JA, Laguerta EP, Ambubuyog G, White RA, Hoblitt RP (1996) Precursory seismicity and forecasting of the June 15, 1991, eruption of Mount Pinatubo. *Fire and Mud: eruptions and lahars of Mount Pinatubo, Philippines*, pp 223–247
- Harris AJL, Baloga S (2009) Lava discharge rates from satellite-measured heat flux. *Geophys Res Lett* 36:L19302. doi:10.1029/2009GL039717
- Harris AJL, Blake S, Rothery DA, Stevens NF (1997) A chronology of the 1991 to 1993 Mount Etna eruption using advanced very high resolution radiometer data: implications for real-time thermal volcano monitoring. *J Geophys Res* 102(B4):7985–8003
- Harris AJL, Flynn LP, Keszthelyi L, Mouginiis-Mark PJ, Rowland SK, Resing JA (1998) Calculation of lava effusion rates from Landsat TM data. *Bull Volcanol* 60:52–71
- Harris AJL, Murray JB, Aries SE, Davies MA, Flynn LP, Wooster MJ, Wright R, Rothery DA (2000) Effusion rate trends at Etna and Krafla and their implications for eruptive mechanisms. *J Volcanol Geotherm Res* 102:237–270
- Harris AJL, Dehn J, Calvari S (2007) Lava effusion rate definition and measurement: a review. *Bull Volcanol* 70:1–22. doi:10.1007/s00445-007-0120-y
- Harris AJL, Steffke A, Calvari S, Spampinato L (2011) Thirty years of satellite-derived lava discharge rates at Etna: implications for steady volumetric output. *J Geophys Res* 116:B08204. doi:10.1029/2011JB008237
- Harris AJL (2013) *Thermal remote sensing of active volcanoes: a user's manual*. Cambridge University Press
- Hooper AJ, Gudmundsson MT, Bagnardi M, Jarosch AH, Spaans K, Magnússon E, Parks M, Dumont S, Ofeigsson B, Sigmundsson F, Hreinsdóttir S, Dahm T, Jonsdóttir, K (2015) Forecasting of flood basalt eruptions: lessons from Bárðarbunga. *AGU Fall Meeting Abstracts*
- Linde AT, Agustsson K, Sacks IS, Stefansson R (1993) Mechanism of the 1991 eruption of Hekla from continuous borehole strain monitoring. *Nature* 365(6448):737–740
- Marzocchi W, Bebbington MS (2012) Probabilistic eruption forecasting at short and long time scales. *Bull Volcanol* 74:1777–1805. doi:10.1007/s00445-012-0633-x
- Marzocchi W, Woo G (2007) Probabilistic eruption forecasting and the call for an evacuation. *Geophys Res Lett* 34:L22310. doi:10.1029/2007GL031922
- Pallister JS, Schneider DJ, Griswold JP, Keeler RH, Burton WC, Noyles C, Newhall CJ, Ratdomopurbo A (2013) Merapi 2010 eruption—chronology and extrusion rates monitored with satellite radar and used in eruption forecasting. *J Volcanol Geotherm Res* 261:144–152
- Pieri D, Abrams M (2005) ASTER observations of thermal anomalies preceding the April 2003 eruption of Chikurachki volcano, Kurile Islands, Russia. *Remote Sens Environ* 99(1):84–94
- Pieri DC, Baloga SM (1986) Eruption rate, area, and length relationships for some Hawaiian lava flows. *J Volcanol Geotherm Res* 30:29–45
- Segall P (2013) Volcano deformation and eruption forecasting. In: Pyle DM, Mather TA, Biggs J (eds) *Remote sensing of volcanoes and volcanic processes: integrating observation and modelling*. *Geol Soc London Spec Pub* 380:85–106. doi:10.1144/SP380.4
- Smets B, Wauthier C, d'Oreye N (2010) A new map of the lava flow field of Nyamulagira (D.R. Congo) from satellite imagery. *J Afr Earth Sci* 58:778–786. doi:10.1016/j.jafrearsci.2010.07.005
- Sparks RSJ (2003) Forecasting volcanic eruptions. *Earth Planet Sci Lett* 210:1–15. doi:10.1016/S0012-821X(03)00124-9
- van Manen SM, Blake S, Dehn J, Valcic L (2013) Forecasting large explosions at Bezymianny Volcano using thermal satellite data. *Geol Soc Lond Spec Publ* 380(1):187–201
- Voight B, Hoblitt RP, Clarke AB, Lockhart AB, Miller AD, Lynch L, McMahon J (1998) Remarkable cyclic ground deformation monitored in real-time on Montserrat, and its use in eruption forecasting. *Geophys Res Lett* 25(18):3405–3408
- Wadge G (1981) The variation of magma discharge during basaltic eruptions. *J Volcanol Geotherm Res* 11:139–168
- Wright R, Blake S, Harris AJL, Rothery DA (2001a) A simple explanation for the space-based calculation of lava eruption rates. *Earth Planet Sci Lett* 192:223–233
- Wright R, Flynn LP, Harris AJL (2001b) Evolution of lava flow-fields at Mount Etna, 27–28 October 1999, observed by Landsat 7 ETM+. *Bull Volcanol* 63:1–7. doi:10.1007/s004450100124
- Wright R, Flynn L, Garbeil H, Harris AJL, Pilger E (2002) Automated volcanic eruption detection using MODIS. *Remote Sens Environ* 82:135–155
- Wright R, Pilger E (2008) Radiant flux from Earth's subaerially erupting volcanoes. *Int J Remote Sens* 29(22):6443–6466. doi:10.1080/01431160802168210
- Wright R, Blackett M, Hill-Butler C (2015) Some observations regarding the thermal flux from Earth's erupting volcanoes for the period of 2000 to 2014. *Geophys Res Lett* 42. doi:10.1002/2014GL061997